Omni-directional Pathloss Measurement Based on Virtual Antenna Array with Directional Antennas

Li, Mengting; Zhang, Fengchun; Zhang, Xiang; Lyu, Yejian; Fan, Wei

Published in:
I E E E Transactions on Vehicular Technology

DOI (link to publication from Publisher):
10.1109/TVT.2022.3210399

Publication date:
2023

Document Version
Accepted author manuscript, peer reviewed version

Omni-directional Pathloss Measurement Based on Virtual Antenna Array with Directional Antennas

Mengting Li, Fengchun Zhang, Xiang Zhang, Yejian Lyu and Wei Fan

***Abstract*—Omni-directional pathloss, which refers to the pathloss when omni-directional antennas are used at the link ends, are essential for system design and evaluation. In the millimeter-wave (mm-Wave) and beyond bands, high gain directional antennas are widely used for channel measurements due to the significant signal attenuation. Conventional methods for omni-directional pathloss estimation are based on directional scanning sounding (DSS) system, i.e., a single directional antenna placed at the center of a rotator capturing signals from different rotation angles. The omni-directional pathloss is obtained by either summing up all the powers above the noise level or just summing up the powers of detected propagation paths. However, both methods are problematic with relatively wide main beams and high side-lobes provided by the directional antennas. In this correspondence, directional antenna based virtual antenna array (VAA) system is implemented for omni-directional pathloss estimation. The VAA scheme uses the same measurement system as the DSS, yet it offers high angular resolution (i.e. narrow main beam) and low side-lobes, which is essential for achieving accurate multipath detection in the power angle delay profiles (PADPs) and thereby obtaining accurate omni-directional pathloss. A measurement campaign was designed and conducted in an indoor corridor at 28-30 GHz to verify the effectiveness of the proposed method.**

***Index Terms*—channel measurements, pathloss, propagation.**

I. Introduction

MILLIMETER wave (mmWave) and sub-Terahertz (THz) frequency bands will continue to play a vital role in the future communication systems since they can provide vast frequency resources to enable high data rate transmission [1], [2]. To achieve optimal system deployment, omni-directional pathloss models which offer flexibility to superimpose arbitrary antenna patterns on the desired propagation scenarios are indispensible for system simulation. However, the omni-directional antennas, especially for those with horizontal polarization, cannot be easily obtained in mmWave and sub-THz bands due to the high design complexity and constrained fabrication accuracy. Besides, omni-directional antennas provide limited link budget in the measurements due to the low antenna gain. This issue becomes more pronounced in mmWave and sub-THz bands owning to the high pathloss. Therefore, the prevalent method to achieve omni-directional pathloss in high frequency bands is to synthesize the omni-pathloss based on directional channel sounding (DSS) [3]–[12] i.e., with a directional antenna placed on a mechanical rotator to capture the signals from different directions.

There are different ways to construct omni-directional pathloss based on DSS. In [6]–[10], the received power of the omni-directional antenna is synthesized by summing up all the power spectrum over delay and angular domain above the noise level. This method is straightforward, but the same paths will be repeatedly counted during the rotation process resulting in underestimation of the omni-directional pathloss due to the wide main beam. In [11], [12], discrete propagation paths are extracted based on the measured results and used to calculate the estimated pathloss by summing up the powers of the identified paths. However, the path identification becomes problematic in angular domain with the non-ideal antenna pattern embeded in the measured frequency response. The omni-directional pathloss is synthesized by first identifying the paths in delay domain and then finding the maximum power at each identified delay bin in power angle delay profile (PADP). With limited delay resolution, the paths with similar delays cannot be totally detected and the omni-directional pathloss might be overestimated. In [13], the power of diffuse paths are considered when approximating the omni-directional pathloss. However, it is still relying on accurate detection of propagation paths at the first step, which cannot be fulfilled by DSS system.

In this correspondence, the omni-directional pathloss is estimated based on a virtual antenna array (VAA) concept with directional antennas instead of the conventional DSS scheme. With high angular resolution and low side-lobes offered by the VAA scheme, the multipath components can be recognized by finding local maxima on PADP and the omni-directional pathloss can be then estimated from the identified paths. The theory of synthesizing the omni-directional path loss is given in Section II. The proposed method is numerically validated in Section III and experimentally validated in Section IV. Finally, a conclusion is drawn in Section V.

II. Omni-directional Pathloss Synthesizing Theory

Assume that a uniform circular array (UCA) consists of P directional antenna elements which are uniformly distributed along a circle with radius of r on the xoy plane, as shown in Fig. 1. The center of the UCA is located at the origin of the coordinate system. The angular position of the p-th element

Mengting Li, Fengchun Zhang, Yejian Lyu and Wei Fan are with the Antenna Propagation and Millimeter-wave Systems (APMS) section, Aalborg University, Denmark.

The work was supported in part by Innovation Fund Denmark under Project 1046-0006, in part by EURAMET European Partnership on Metrology Programme (MEWS), and in part by European COST INTERACT Action under Grant CA20120.

Xiang Zhang is with China Academy of Information and Telecommunications Technology (CAICT), Beijing 100191, China

Corresponding author: Wei Fan (Email: wfa@es.aau.dk).

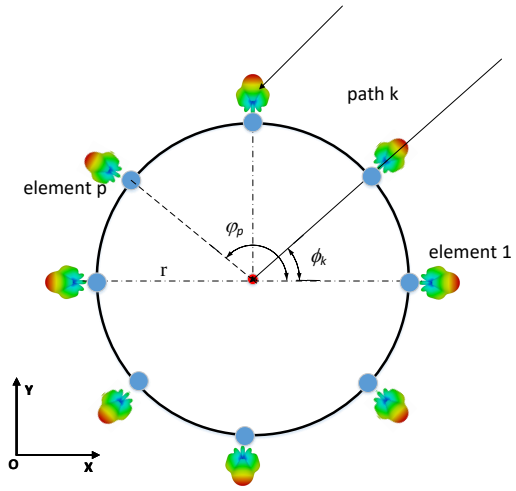

Fig. 1. A diagram of the UCA and the propagation channel.

is $\varphi_p = 2\pi \cdot (p-1)/P, p \in [1, P]$. The frequency band is within the range of $[f_L,\ f_U]$ with f_L and f_U denoting the lower and the upper frequencies, respectively. Suppose there are K plane waves impinging on the UCA with the k-th path from direction ϕ_k. The multipath in our measurements given in Section IV is mainly confined in the azimuth plane since the transmit and receive antennas are placed in the same height and the receive antenna has narrow beamwidth in the E-plane. Therefore, the discussion here is limited to a 2-D model, i.e. with the multipath and the UCA confined in the UCA plane (xoy plane herein). Note that it is possible to extend the present model into a 3-D model. We assume that all the virtual array elements receive the same signal power for a specific multipath ignoring the deviation caused by the array aperture. The errors introduced by the assumption are negligible when the path length is far larger than the radius of the UCA. The channel frequency response (CFR) at the p-th UCA element can be expressed as

$$H_p(f) = \sum_{k=1}^{K} \alpha_k \exp(-j2\pi f \tau_k) \ \cdot a_p(f, \phi_k), \tag{1}$$

where α_k and τ_k represent the complex amplitude and delay of the k-th path ($k \in [1, K]$), respectively. $a_p(f, \phi_k)$ is the transfer function between the k-th path and the p-th array element, which is normalized by that between the k-th path and UCA center, expressed as

$$a_p(f, \phi_k) = \exp(\frac{j2\pi fr}{c} cos(\phi_k - \varphi_p)) g(f, \phi_k - \varphi_p), \tag{2}$$

where c is the speed of light. $g(f, \phi)$ is the 2-D complex radiation pattern (antenna gain is normalized to 1 for the ease of calculation) of the antenna element at xoy plane with its boresight direction along x axis.

Using the modified classical beamforming proposed in [14], the steering weight of the p-th array element can be written as

$$\omega_p(f, \phi) = \exp[-\frac{j2\pi fr}{c} cos(\phi - \varphi_p)] \cdot s(\phi), \tag{3}$$

where $s(\phi)$ is the window function which is define by

$$s(\phi) = \begin{cases} 0, \mid \phi - \varphi_p \mid > B \\ 1, \mid \phi - \varphi_p \mid \leqslant B, \end{cases} \tag{4}$$

where B is the selected angle range and the phase of $(\phi - \varphi_p)$ is wrapped within $(-180°, 180°)$. To include sufficient array elements and suppress the sidelobes, the angle range B can be selected as 90°. The modified classical beamforming result can be obtained by

$$Q(f, \phi) = \sum_{p=1}^{P} \omega_p(f, \phi) \cdot H_p(f) \ . \tag{5}$$

It can also be expressed as a summation of the beam patterns of the K paths by taking (1) into (5):

$$\begin{aligned} Q(f, \phi) &= \sum_{k=1}^{K} \alpha_k \exp(-j2\pi f \tau_k) \ \sum_{p=1}^{P} a_p(f, \phi_k) \cdot \omega_p(f, \phi) \\ &= \sum_{k=1}^{K} \alpha_k \exp(-j2\pi f \tau_k) \cdot \upsilon_k(f, \phi) \ , \end{aligned} \tag{6}$$

where $\upsilon_k(f, \phi)$ represents the array beam pattern of the k-th path with modified classical beamforming and $\mid \upsilon_k(f, \phi_k) \mid^2$ is the array gain. The PADP with modified classical beamforming can be obtained via inverse Fourier transformation:

$$\begin{aligned} q(\tau, \phi) &= \sum_{f=f_L}^{f_U} Q(f, \phi) \cdot \exp(j2\pi f \tau) \\ &= \sum_{k=1}^{K} \sum_{f=f_L}^{f_U} \upsilon_k(f, \phi) \cdot \alpha_k \exp[-j2\pi f(\tau - \tau_k)]. \end{aligned} \tag{7}$$

In the proposed method, $\upsilon_k(f, \phi)$ with a narrower beamwidth and lower side-lobes can be formed, which can mimic the Dirac delta function better and the multipaths can be identified as local peaks of the PADP. This 2-D peak identification is performed by firstly finding local maxima of power delay profile (PDP) curves [15]. Similar peak detection is also performed on angular domain at the identified delays. The estimated multipath is denoted by

$$\mathcal{P} = \{\phi_k, \tau_k, P_k\}_{k=1}^{K}, \tag{8}$$

where P_k is the estimated power of the k-th path received by virtual UCA.

In the ideal case, i.e., the transmitting (Tx) and receiving (Rx) antennas are both omni-directional antennas, the omni-directional pathloss is calculated by subtracting the summed received power from the transmit power (unit: dBm) with the Tx and Rx antenna gains removed from the received path power (to provide the equivalent 0 dB antenna gain for both Tx and Rx sides). That is, we are interested in the omni-directional pathloss of the propagation channel, with antenna effects removed. The transmit power is assumed as 0 dBm for the pathloss calculations in the following discussions. The omni-directional pathloss can be then derived by

$$PL_{ideal} = -10\log_{10}(\sum_{k=1}^{k=K}\frac{\hat{P}_k}{G_{tx}\cdot G_{rx}}), \tag{9}$$

where $\hat{P}_k$ is the received power of the k-th path at the Rx side. G_{tx} and G_{rx} are the gains of transmitting omni-directional antenna and receiving omni-directional antenna, respectively.

In the proposed method, either the Tx omni-directional antenna or the Rx omni-directional antenna can be substituted by the directional antenna based VAA. For the case with VAA serving as Tx antenna, the equation used for estimating omni-directional pathloss can be updated by

$$PL_{omni} = -10\log_{10}(\sum_{k=1}^{k=K}\frac{P_k}{G_{rx}\cdot G_{vaa}(k)}), \tag{10}$$

where G_{rx} and $G_{vaa}(k) = \mid \upsilon_k(f,\phi_k) \mid^2$ represent the gain of Rx omni-directional antenna and the combined virtual array gain, respectively. Note that the array gain at center frequency is generally used for calculation and we have $G_{vaa}(1) = G_{vaa}(2) = \cdots = G_{vaa}(K)$ due to the symmetrical UCA configuration for different paths. For UCA, the beam pattern is consistent for different beam-steering angles.

The main formulas of two reference methods mentioned in the Introduction, i.e., [6]-[10] denoted as Ref 1 and [11], [12] denoted as Ref 2, are also given here for comparison. These two reference methods are both based on DSS. Suppose that the CFR measured by DSS scheme at the m-th rotation angle ($1 \leqslant m \leqslant M$) is denoted by $\tilde{H}_m(f)$. The angular dependent channel impulse response (CIR) $\tilde{h}(l,m)$ is derived by the inverse Fourier transform of $\tilde{H}_m(f)$, where l represents the l-th delay bin ($1 \leqslant l \leqslant L$). The PADP using DSS can be obtained from $\left|\tilde{h}\,(l,m)\right|^2$.

For Ref 1, the omni-directional pathloss is calculated by summing up all the powers in PADP above the noise level:

$$PL_{Ref1} = -10\log_{10}(\sum_{l=1}^{l=L}\sum_{m=1}^{m=M}\frac{\mid \hat{h}(l,m) \mid^2}{G_1\cdot G_2}), \tag{11}$$

where $\hat{h}(l,m)$ represents the de-noised CIR. G_1 and G_2 represent the gain of the Tx antenna and Rx antenna used in the DSS system, respectively. Note that the directional antenna can serve as either Rx or Tx antenna.

For Ref 2, the pathloss is calculated by summing up the powers of identified propagation paths in PADP. The delays of the identified paths are obtained from the 1-D local maxima search on the PDP [15]. The index of the delay bin of the identified multipath is denoted as $\tilde{l}_k$ ($1 \leqslant k \leqslant K$). The power of the k-th path received by Rx antenna using DSS is estimated by $\tilde{P}_k = \max\limits_{1\leqslant m\leqslant M}\left|\tilde{h}\left(\tilde{l}_k,m\right)\right|^2$. The omni-directional pathloss using Ref 2 is then derived by

$$PL_{Ref2} = -10\log_{10}(\sum_{k=1}^{k=K}\frac{\tilde{P}_k}{G_1\cdot G_2}). \tag{12}$$

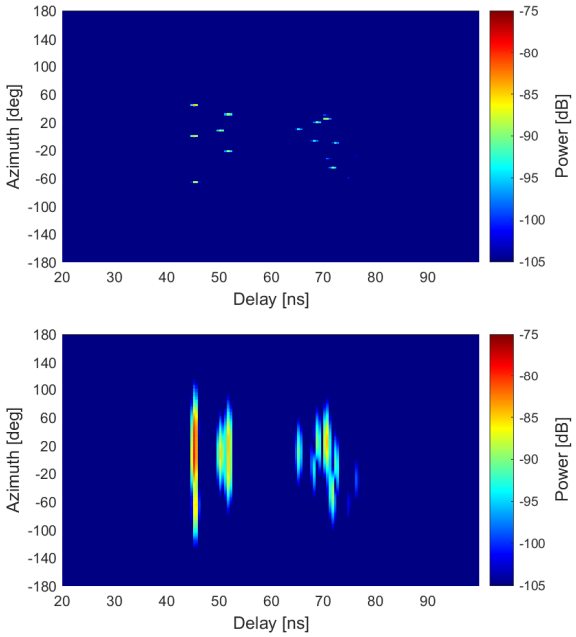

Fig. 2. Simulated PADPs obtained by (a) VAA and (b) DSS schemes.

III. Simulation Validation

In the simulation, the virtual UCA consists of 360 equally distributed elements with a radius of 0.25 m. The measured pattern of corrugated antenna with 40° HPBW and 13.5 dBi gain at 29 GHz was used as element pattern for the virtual array [16]. As a comparison, the DSS scheme is also simulated using the measured antenna pattern. The frequency band is from 28-30 GHz with 1001 frequency points. A representative multipath scenario with 20 paths is considered here. The powers of these paths at the receiver side are between -80 to -105 dB with a delay range of 45 ns to 80 ns.

PADPs obtained by DSS and VAA schemes are shown in Fig. 2 (a) and (b), respectively. The parameters of these paths are deliberately designed, i.e. with either close delays or similar angle of arrivals (AOAs) to form a critical scenario as seen in Fig. 2. Compared with the DSS scheme, the angular resolution can be significantly improved using VAA scheme. Therefore, the proposed method can provide better capabilities in distinguishing the multipath. Based on the results of PADPs, the omnidirectional pathloss is calculated using Ref 1, Ref 2 and the proposed method. The true value of the omni-directional pathloss with the pre-set 20 multipath is 74.43 dB whereas the omni-directional pathloss results estimated by Ref 1, Ref 2 and the proposed method are 71.03 dB, 76.57 dB and 75.03 dB, respectively. Ref 1, Ref 2 and the proposed method have a deviation of 3.4 dB, 2.14 dB and 0.6 dB from the true value, respectively. The omnidirectional pathloss estimated by Ref 1 is larger than the true-value since same paths could be counted repeatedly at different angles. The result of Ref 2 is below the true value since only the path with maximum power is counted at the identified delay bins.

There is still 0.6 dB estimation error for the proposed method, though the error is much smaller than the reference methods. The reason is that the synthesized virtual array

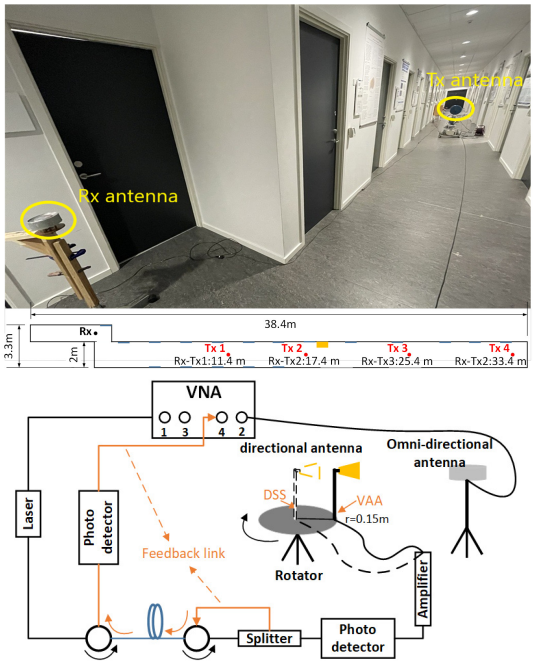

Fig. 3. The photo of the measurement scenario (above) and the diagram of the measurement system (below).

pattern cannot be an ideal pattern with infinitely narrow beamwidth and infinitely low sidelobe level, resulting in estimation errors. The errors can be further reduced using VAA with a larger array size, but it will also increase the number of the array elements and the measurement time. Nevertheless, the proposed method with more directional antenna pattern is closer to ideal pencil beam case, leading higher angular resolution of the multiple paths and less energy leakage from other paths. The improvement of the proposed method might vary in different scenarios. However, the proposed VAA scheme is expected to show its priority for propagation scenario with many cluster-like multipaths.

IV. Measurement Validation

A. Measurement Campaign

The measurements were conducted in an indoor corridor at Aalborg University, as shown in Fig. 3. We have conducted four measurement campaigns in static propagation environments, i.e., the characteristics of the multipath will not change over time. Therefore, only one channel snapshot measurement was required to characterize the channel. The Rx antenna was located at a corner of the building where the line-of-sight (LOS) rays were blocked by walls and the Tx antenna was moved along the corridor to the location of Tx 1, 2, 3, 4 with a link distance of 11.4 m, 17.4 m, 25.4 m, 33.4 m, respectively (as shown in the Fig. 3 (above)). The Rx and Tx antennas were both placed over the ground with a height of 93 cm. Note that the measurement campaigns are designed only for validating the proposed method. Characterizing omni-directional pathloss for different deployment scenarios will be considered in the future. The measurement system is illustrated in Fig. 3 and its working principle is detailed in [17]. This VNA-based channel sounder can support long range phase-coherent measurements in the mm-Wave bands by using optical fiber cables and the phase compensation scheme. In VNA-based channel measurements, CFR is obtained from the measured S21 over the selected frequency band.

As illustrated in Fig. 3 (below), both the DSS measurements, i.e., with the directional antenna placed at the rotation center, and the proposed directional antenna based VAA measurements, i.e., with the directional antenna placed with a certain distance from the rotation center were conducted. The DSS measurements and its result analysis are used for comparison. The Rx antenna is a vertically polarized biconical antenna [18], which has almost omni-directional radiation pattern in the azimuth plane (with around 2 dB ripple over 360 degrees) and a 5.5 dBi gain at 29 GHz. The corrugated antenna [16] with 40° HPBW and 13.5 dBi gain at 29 GHz is selected as the Tx antenna fixed on the mechanical rotator since it can form a VAA with high angular resolution as validated in [14]. The corrugated antenna was rotated automatically over the whole azimuth plane with a rotation step of 1.5° (i.e. 240 steps in total) for both the DSS and VAA measurements. The measured frequency range is from 28 to 30 GHz with 1001 frequency points for each rotation angle. Given the 2 GHz frequency bandwidth, the delay resolution in our measurement is 0.5 ns, resulting in a spatial resolution of 0.15 m. With 1001 frequency points, the delay range of the measurement is 500 ns and the maximum measurement range is 150 m path length. For VAA measurements, the corrugated antenna was placed 0.15 m away from the rotation center to form a virtual UCA. As described, the measurement system and measurement time for the DSS and VAA schemes are the same.

B. Measurement Results

1) Power Angle Delay Profile: For simplicity, only PADPs with link distance of 17.4 m are given here as examples. The PADPs obtained from VAA and DSS scheme are depicted in Fig. 4 (a) and Fig. 4 (b), respectively. The multipath distributes in a wide angular and delay ranges due to the high-order bounces caused by the walls. It can be clearly seen in Fig. 4 (b) that, different paths are overlapped with each other due to the wide main beam of the antenna. Compared with DSS, the PADP obtained from VAA provides much higher angular resolution and the multipath becomes easier to be recognized.

2) Omni-directional Pathloss: Fig. 5 depicts the estimated omni-directional pathloss using the proposed method and two reference methods. As discussed earlier, with the proposed method, the multipath can be more accurately detected by finding local maximum peaks in both angular and delay bins. The estimated pathloss obtained from Ref 1 is always below the proposed method with a maximum value of 3.9 dB in the measured scenarios. The reason is that the same paths are counted repeatedly at different rotation angles. The estimation difference between Ref 2 and the proposed method reaches 4 dB in the scenario with the largest link distance. The pathloss is overestimated using Ref 2 since its capability of identifying multipath is constrained by the non-ideal antenna pattern. Only the path with maximum power is counted at the identified

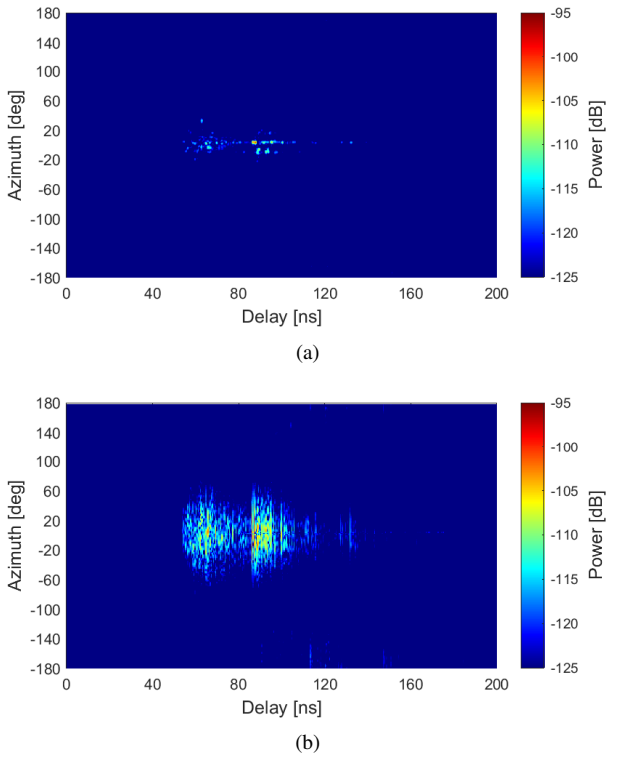

Fig. 4. PADP obtained from (a) VAA and (b) DSS schemes with link distance of 17.4 m.

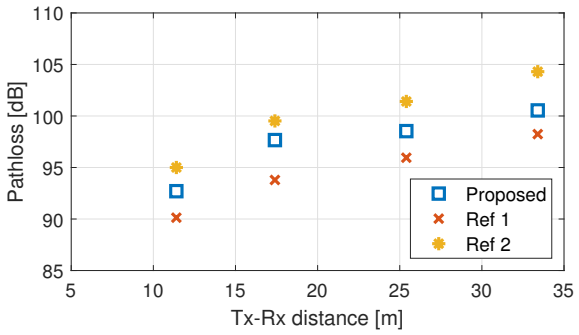

Fig. 5. The estimated omni-directional pathloss at 29 GHz using conventional methods and the proposed method.

delay bins in this case. Overall, the pathloss calculated from the proposed method is always between the pathloss obtained from two reference methods, as expected.

V. Conclusion

A new approach of estimating the omni-directional pathloss is presented in this correspondence. Directional antenna based VAA is used to achieve high angular resolution and reduce the side-lobe effects on the PADP. Compared with the traditional DSS method, the propagation paths are more accurately identified with VAA scheme by searching local maxima in the PADP, without introducing additional cost and increasing the measurement time. In the simulation, the proposed method only has 0.6 dB estimation errors whereas Ref 1 and Ref 2 have 3.4 dB and 2.14 dB errors, respectively. The measured results show that the omni-directional pathloss estimated by the proposed method is always between the results of Ref 1 and 2, which matches expectations. As observed, the estimation errors introduced by non-ideal antenna patterns using DSS method are not negligible. The proposed method can provide a more accurate path detection and improve the omni-directional pathloss estimation results.

References

[1] T. S. Rappaport, S. Sun, R. Mayzus, H. Zhao, Y. Azar, K. Wang, G. N. Wong, J. K. Schulz, M. Samimi, and F. Gutierrez, "Millimeter wave mobile communications for 5G cellular: It will work!" *IEEE access*, vol. 1, pp. 335–349, 2013.

[2] V. Degli-Esposti, F. Fuschini, E. M. Vitucci, M. Barbiroli, M. Zoli, L. Tian, X. Yin, D. A. Dupleich, R. Müller, C. Schneider *et al.*, "Ray-tracing-based mm-wave beamforming assessment," *IEEE Access*, vol. 2, pp. 1314–1325, 2014.

[3] C. Gustafson, K. Haneda, S. Wyne, and F. Tufvesson, "On mm-wave multipath clustering and channel modeling," *IEEE Transactions on Antennas and Propagation*, vol. 62, no. 3, pp. 1445–1455, 2013.

[4] C. Ling, X. Yin, R. Müller, S. Häfner, D. Dupleich, C. Schneider, J. Luo, H. Yan, and R. Thomä, "Double-directional dual-polarimetric cluster-based characterization of 70–77 ghz indoor channels," *IEEE Transactions on Antennas and Propagation*, vol. 66, no. 2, pp. 857–870, 2017.

[5] R. He, C. Schneider, B. Ai, G. Wang, Z. Zhong, D. A. Dupleich, R. S. Thomae, M. Boban, J. Luo, and Y. Zhang, "Propagation channels of 5g millimeter-wave vehicle-to-vehicle communications: Recent advances and future challenges," *IEEE vehicular technology magazine*, vol. 15, no. 1, pp. 16–26, 2019.

[6] M. Kyro, K. Haneda, J. Simola, K. Nakai, K.-i. Takizawa, H. Hagiwara, and P. Vainikainen, "Measurement based path loss and delay spread modeling in hospital environments at 60 GHz," *IEEE Transactions on Wireless Communications*, vol. 10, no. 8, pp. 2423–2427, 2011.

[7] M. R. Akdeniz, Y. Liu, M. K. Samimi, S. Sun, S. Rangan, T. S. Rappaport, and E. Erkip, "Millimeter wave channel modeling and cellular capacity evaluation," *IEEE journal on selected areas in communications*, vol. 32, no. 6, pp. 1164–1179, 2014.

[8] S. Sun, G. R. MacCartney, M. K. Samimi, and T. S. Rappaport, "Synthesizing omnidirectional antenna patterns, received power and path loss from directional antennas for 5g millimeter-wave communications," in *2015 IEEE Global Communications Conference (GLOBECOM)*. IEEE, 2015, pp. 1–7.

[9] G. R. Maccartney, T. S. Rappaport, S. Sun, and S. Deng, "Indoor office wideband millimeter-wave propagation measurements and channel models at 28 and 73 GHz for ultra-dense 5G wireless networks," *IEEE access*, vol. 3, pp. 2388–2424, 2015.

[10] F. Fuschini, S. Häfner, M. Zoli, R. Müller, E. Vitucci, D. Dupleich, M. Barbiroli, J. Luo, E. Schulz, V. Degli-Esposti *et al.*, "Analysis of in-room mm-wave propagation: Directional channel measurements and ray tracing simulations," *Journal of Infrared, Millimeter, and Terahertz Waves*, vol. 38, no. 6, pp. 727–744, 2017.

[11] S. Hur, Y.-J. Cho, J. Lee, N.-G. Kang, J. Park, and H. Benn, "Synchronous channel sounder using horn antenna and indoor measurements on 28 GHz," in *2014 IEEE International Black Sea Conference on Communications and Networking (BlackSeaCom)*. IEEE, 2014, pp. 83–87.

[12] S. Hur, Y.-J. Cho, T. Kim, J. Park, A. F. Molisch, K. Haneda, and M. Peter, "Wideband spatial channel model in an urban cellular environments at 28 GHz," in *2015 9th European conference on antennas and propagation (EuCAP)*. IEEE, 2015, pp. 1–5.

[13] K. Haneda, S. L. H. Nguyen, J. Järveläinen, and J. Putkonen, "Estimating the omni-directional pathloss from directional channel sounding," in *2016 10th European Conference on Antennas and Propagation (EuCAP)*. IEEE, 2016, pp. 1–5.

[14] M. Li, F. Zhang, Y. Ji, and W. Fan, "Virtual antenna array with directional antennas for millimeter-wave channel characterization," *IEEE Transactions on Antennas and Propagation*, 2022.

[15] K. Haneda, J. Järveläinen, A. Karttunen, M. Kyrö, and J. Putkonen, "A statistical spatio-temporal radio channel model for large indoor environments at 60 and 70 ghz," *IEEE Transactions on Antennas and Propagation*, vol. 63, no. 6, pp. 2694–2704, 2015.

[16] A. S. S. (ASYSOL), "Data sheet for asy-cwg-s-265." 2021, accessed 4 March 2021. [Online]. Available: https://asysol.com/portfolio/circular-corrugated-feeds/

[17] A. W. Mbugua, W. Fan, K. Olesen, X. Cai, and G. F. Pedersen, "Phase-compensated optical fiber-based ultrawideband channel sounder," *IEEE Transactions on Microwave Theory and Techniques*, vol. 68, no. 2, pp. 636–647, 2019.

[18] A-INFO, "Data sheet for biconical antenna sz-2003000/p." 2021, accessed 4 March 2021. [Online]. Available: https://www.ainfoinc.com/antenna-products/bi-conical-antennas/sz-2003000-p-bi-conical-antenna-2-30-ghz-0db-gain-sma-female